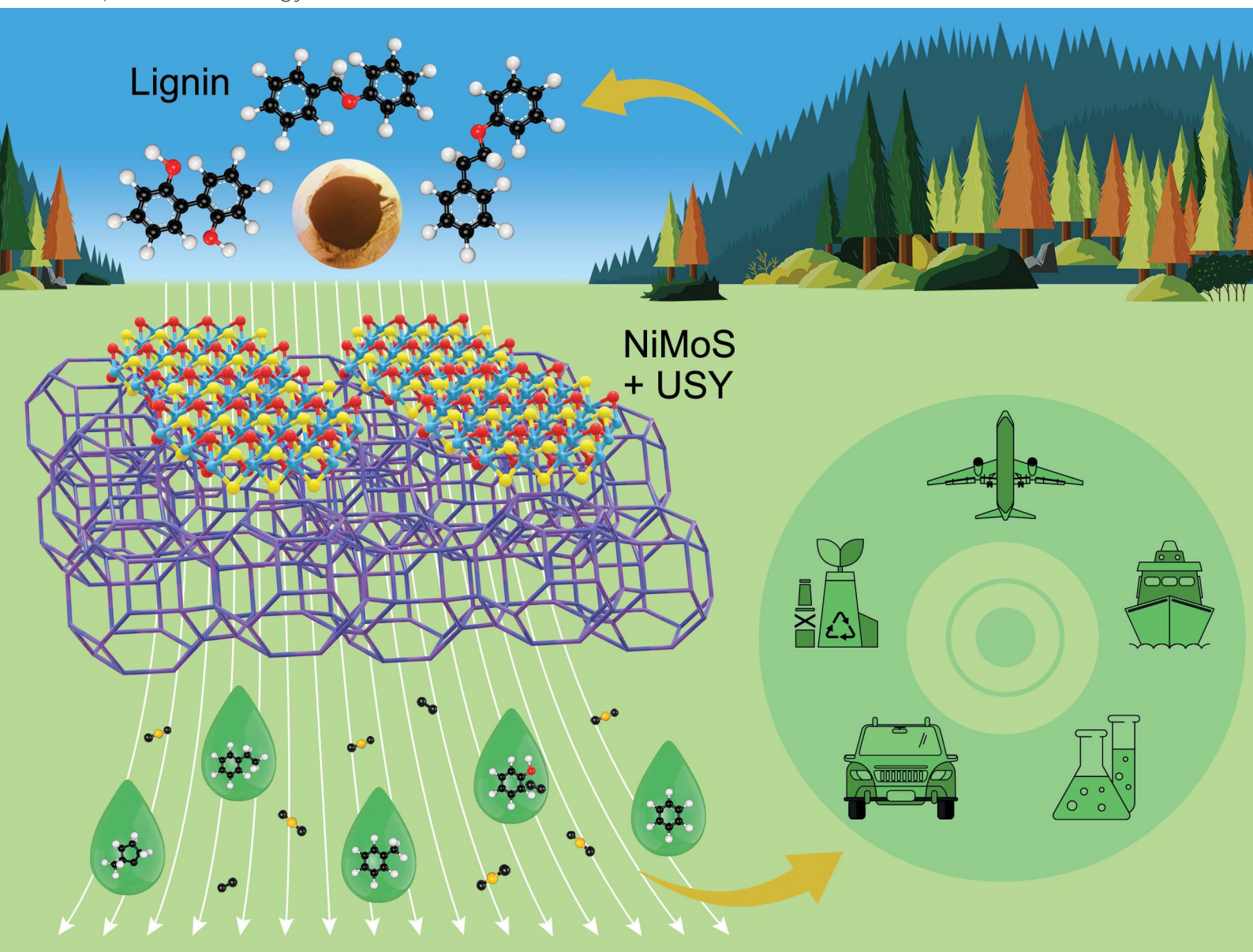


Sustainable Energy & Fuels

Interdisciplinary research for the development of sustainable energy technologies

rsc.li/sustainable-energy



ISSN 2398-4902


PAPER

Louise Olsson *et al.*
NiMoS on alumina-USY zeolites for hydrotreating lignin
dimers: effect of support acidity and cleavage of C–C bonds



Cite this: *Sustainable Energy Fuels*, 2020, 4, 149

NiMoS on alumina-USY zeolites for hydrotreating lignin dimers: effect of support acidity and cleavage of C–C bonds†

Muhammad Abdus Salam,^{ab} Prakhar Arora,^a Houman Ojagh,^a You Wayne Cheah,^a Louise Olsson ^{*a} and Derek Creaser^a

NiMoS on alumina, USY and mixed alumina-USY supports was studied in a batch reactor to assess the effect of support acidity in valorizing lignin dimers by hydrodeoxygenation (HDO). The reactivity of α -O-4 (benzyl phenyl ether), β -O-4 (2-phenethyl phenyl ether) and 5-5' (2,2'-dihydroxybiphenyl) linkages was investigated in dodecane at 593 K and a H₂ pressure of 5 MPa. A relatively fast rate of hydrogenolysis of the sp³ hybridized etheric bonds was observed for the catalyst supported on the mixed support. With the α -O-4 linkage, the USY supported catalyst selectively yielded deoxygenated aromatics including BTX products with fewer residual C-C dimers. For the β -O-4 linkage, analogous trends have been observed but with more aromatics. Interestingly, with 5-5' linkages the catalyst on USY and mixed supports can break the C-C linkages without producing other intermediate C-C dimer byproducts. The results show high hydrocracking and isomerization activities of the catalyst supported on USY and mixed supports. This is consistent with XRD, Raman, XPS and TEM measurements, where enhanced dispersion of the active phase was observed. However, hydrogenation activity on the USY support is reduced to a significant degree which results in a large amount of benzene compared to NiMoS-Al₂O₃ that produces mostly cyclohexane. In addition, elemental analysis revealed that carbon deposition is higher on the USY-based catalyst compared to the alumina-based catalyst owing to its higher acidity. However, the potential for superior C-C bond cleavage on NiMoS-USY opens the possibility to valorize technical lignin in biorefinery processes.

Received 14th July 2019
Accepted 7th October 2019

DOI: 10.1039/c9se00507b

rsc.li/sustainable-energy

Introduction

Lignin, an integral part of lignocellulosic materials, is a three-dimensional cross-linked bio-polymer consisting of three different phenylpropane units linked *via* ether and C–C bonds.¹ Such heterogeneity makes it recalcitrant to depolymerization and further upgrading processes. Nonetheless, it is highly rich in aromatics with aliphatic moieties and offers huge potential for utilization as a renewable feedstock despite its current treatment that is largely as a waste or use for low value applications in existing biorefineries. In recent years, lignin and lignin derived feedstocks have received substantial research focus for producing green chemicals and fuels. Lignin derived bio-oil primarily contains alkyl or methoxy substituted phenols including phenolic dimers, trimers and oligomers with residual C–C and C–O–C linkages from the original lignin structure.² The

oxygenates thus present in bio-oil (40–45%) have detrimental properties (*e.g.* coke precursors) that impede its direct utilization.^{3,4} Hence an efficient upgrading process must achieve simultaneous breakdown of these linkages and subsequent processing with a robust catalyst to produce specialty chemicals and stable bio-fuels. Among many processes, catalytic hydrodeoxygenation (HDO) is unique because it offers the possibility to perform depolymerization and deoxygenation concurrently.

Several catalysts (mono-bimetallic and bifunctional) containing noble metals (Pt, Pd, Rh, Ru, Re, and Ir), metal-sulfides, carbides, nitrides, and phosphides of various supports (carbon, Al_2O_3 , ZrO_2 , TiO_2 , $\text{ZrO}_2\text{-SiO}_2$, $\text{SiO}_2\text{-Al}_2\text{O}_3$, zeolites, mesoporous silicates, *etc.*) have been studied extensively for HDO of phenols,⁵⁻¹² anisole,^{9,13-16} substituted phenols (cresols, guaiacols, syringols, eugenols, *etc.*)^{6,9,17-30} and lignin dimers.³¹⁻³⁶ The product distribution exclusively depends on the physicochemical properties of the chosen catalyst-support system and the employed reaction conditions. The high hydrogenation (HYD) activity of the precious metals typically leads to aromatic ring HYD followed by acid catalyzed dehydration to cycloalkanes in the gasoline ($\text{C}_6\text{-C}_9$) range.^{6,37} Nevertheless, by tuning the intrinsic energy barriers for HYD *versus* direct deoxygenation (DDO) on different surfaces one can alter the selectivity to bio-

*“Competence Centre for Catalysis, Department of Chemistry and Chemical Engineering, Chalmers University of Technology, SE-41296, Gothenburg, Sweden.
E-mail: louise.olsson@chalmers.se*

^bShahjalal University of Science and Technology, Sylhet-3114, Bangladesh

† Electronic supplementary information (ESI) available. See DOI: 10.1039/c9se00507b

arenes.^{14,21} But noble metals are not stable in the presence of sulfur which makes them less favorable for upgrading Kraft (1–3 wt% S) and lignosulfonate (4–8 wt% S) lignin.³⁸ Also, the cost of such metals hinders scale up.³⁵ Transition metals, *e.g.* Co or Ni promoted MoS₂, commonly used for hydro-desulfurization (HDS) and hydro-denitrogenation (HDN) favor a consecutive DDO-HYD route during HDO to yield a mixture of alicyclics and aromatics, hence retaining the aromaticity partially or fully. Recently, Song *et al.*³⁹ claimed that unsupported CoMoS nano-sulfides are efficient in converting monophenols and diphenyl ether to aromatics.

For lignin dimers having α -O-4 or β -O-4 linkages, sp³ hybridized C_{aliphatic}-O cleavage is rather fast compared to that of the resonance stabilized sp² C_{aromatic}-O linkages and this initially yields mono- and substituted phenols or mono-aromatics in the presence of H₂. Hydrocracking of lignin dimers on sulfided NiMo-Al₂O₃ by Koyama *et al.*³² showed the formation of substantial amounts of monoaromatics and dimers. However, lignin from the paper and pulp industry or other biorefineries, referred to as 'technical lignin', would also require cleavage of their condensed C-C linkages to catalyze their conversion to chemicals or fuels. Very few catalysts are reported to break these β -1, β - β , β -5, and 5-5' bonds as they require a higher bond dissociation energy. Shuai *et al.*⁴⁰ reported selective cleavage of a C-C bond in a lignin dimer (dimethylguaiacylmethane) to two phenolic monomers while DPM (diphenyl methane), an aromatic dimer, did not convert. Hence, a catalyst capable of efficiently cleaving both C-C and C-O-C linkages would be ideal for valorizing lignin to specialty chemicals and fuels.⁴¹ In this context, NiMoS on mixed alumina and ultra-stable Y zeolites was studied here with the aim to understand the physicochemical properties related to metal function and Brønsted acidity for cleavage of both C-O-C and C-C linkages present in lignin dimers.

It is well known that the support composition, type, acidity and support-metal interaction play a dynamic role in determining catalytic activity.⁴² The tangible challenges with zeolites are the textural properties of the support which include pore accessibility, diffusion barriers for the reactants and products, acidity of the catalyst and deactivation by coking.^{8,43} Compared to ZSM-5 and beta zeolites, USY zeolite has a large pore size (7.4 Å), and higher thermal and hydro-thermal stability.^{44,45} Previous studies with NiMoS on modified or mesoporous USY have been explored for hydrogenation, hydrocracking, and ring opening reactions for heavy vacuum gas oil (HVGO)/light cycle oil (LCO).^{46–49} The morphologies of the MoS₂ phase, as well as the vicinity and the strength of the acid sites are vital for such upgrading. Hydrogen spillover and better metal (Pd) dispersion on 20% HY (Si/Al = 2.3) and Al₂O₃ were reported to be beneficial for high phenol HDO.⁸ Hong *et al.*⁵⁰ studied phenol HDO over Pt/HY and observed hydrogenation-hydrogenolysis ring coupling to yield mono- and bicyclic hydrocarbons. Lee *et al.*⁵¹ reported that higher acidity increases guaiacol conversion and enhances deoxygenation. Other studies include non-metallic USY for lignin depolymerization to phenolics/aromatics.⁵²

However, there are to our knowledge no studies available where NiMoS on USY or alumina modified USY is used for hydrotreatment of lignin dimers, which is the objective of the current work. In more detail we have studied hydrotreating of three major lignin linkages, presented in Fig. 1. In addition, we have performed detailed characterization using Raman spectroscopy, XPS, TEM, XRD, TPD, BET and elemental analysis to correlate our results with the catalyst composition.

Experimental

Catalyst preparation

Ni and Mo containing catalysts were prepared by a wet impregnation process using pre-calcined γ -alumina and ultra-stable Y-zeolite (Si/Al = 15, Zeolyst International). Ammonium molybdate tetrahydrate (81–83% MoO₃ basis, Sigma-Aldrich) and nickel(II) nitrate hexahydrate (98%, Sigma-Aldrich) were used as the metal precursors. Three different catalysts namely NiMo on γ -alumina (NiMoA), NiMo on USY-zeolite (NiMoY) and NiMo on a mixed support consisting of equal amounts of γ -alumina and USY-zeolite (NiMoAY) were synthesized. The details of the catalyst synthesis have been described elsewhere.^{53–55}

Catalytic activity measurements

The catalyst was sulfided using dimethyl disulfide ($\geq 99.5\%$, Sigma-Aldrich) at 613 K and 2.5 MPa of hydrogen (99.9%, AGA) in a Parr autoclave reactor (300 ml, Parr Inc.) before each activity test. The feed consisted of lignin model compounds, namely 5 mol% benzyl phenyl ether (98%, Sigma Aldrich), 5 mol% 2-phenethyl phenyl ether (98%, Frinton Laboratories Inc.) or 1.8 mol% 2,2'-biphenol (99%, Sigma Aldrich) each in dodecane ($\geq 99\%$, Sigma Aldrich).

In each experiment, 0.5 g of the catalyst was used. After loading the reactor with the catalyst, solvent and reactant, it was flushed three times with N₂ and H₂ respectively. It was then pressurized to 1 MPa using H₂ at room temperature and rapidly heated up to 593 K. The final pressure of the reactor was maintained at 5 MPa of H₂ with a stirring rate of 1000 rpm. Samples were collected during the reaction at 35, 60, 120, 180, 240, 300 and 360 min to analyze the liquid composition. Each sample withdrawal caused a temporary pressure-drop of *ca.* 0.1–0.2 MPa in the reactor which was compensated for *via* adding H₂ immediately to return to 5 MPa. After 6 h, the reaction was stopped by rapid cooling, and the catalyst was recovered and washed with diethyl ether to remove the adhering reactants, residual products, and intermediates. The catalyst was then dried and analyzed.

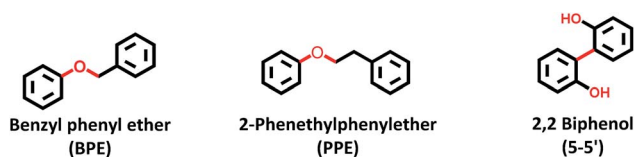


Fig. 1 Lignin model compounds used to mimic ether and C-C linkages.



Sustainable Energy Fuels, 2020, 4, 149–163 | 151

number of Mo atoms at the edge of one MoS₂ slab which can be determined from its length, $L = 3.2(2n_i - 1) \text{ \AA}$, and m is the total number of slabs.

Results and discussion

HDO of BPE

Fig. 2 presents the products and intermediates formed during the HDO of BPE. Selective hydrogenolysis of the C_{aliphatic}-O bond (α -O-4) in BPE primarily yields toluene and phenol.⁵⁷ On the other hand, the acid catalyzed transalkylation reaction *via* the transfer of the benzyl group in BPE leads to the formation of benzyl phenols.¹³ As reported in the literature, recombination of hydrogenolysis and hydrolysis intermediates may also form benzyl phenols and other dimers linked *via* C-C bonds as

presented in Fig. 2(c).³⁴ However, transalkylation seems to be the dominant path to form benzyl phenols as the peak in their formation coincides with when full conversion of BPE occurs. Fig. 2(c) illustrates all the components identified by GC-MS analysis of the samples in a proposed reaction scheme. It is important however to note that benzyl alcohol (faint print in Fig. 2(c)) was not detected. This suggests that the recombination pathway is of lesser importance or that benzyl alcohol is rapidly consumed when formed. The catalysts containing Y-zeolite have enhanced rates of hydrogenolysis as shown in Fig. 2(a). Approximately, 80–90% conversion of BPE occurs in 0.5 h for catalysts with Y-zeolite. This is likely due to increased rates of the transalkylation and hydrolysis reactions of BPE with the more acidic catalysts. The phenolics thus formed undergo HDO, HYD, isomerization and hydrocracking to yield a mixture

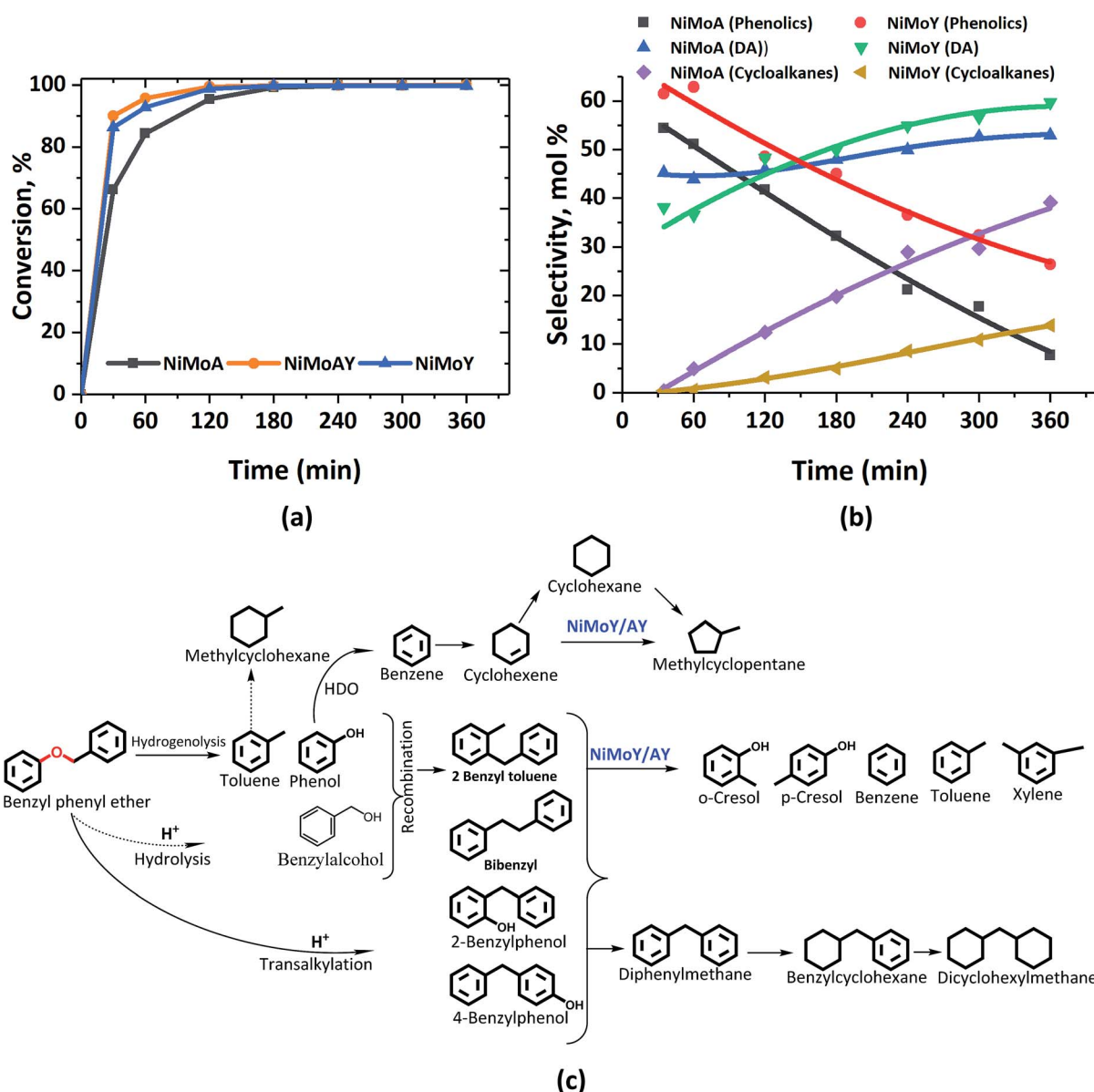


Fig. 2 (a) BPE conversion and (b) product selectivity during HDO of BPE in an autoclave at 593 K, 5 MPa and 1000 rpm. (c) Proposed reaction scheme. DA = deoxygenated aromatics.



of deoxygenated aromatics and alicyclics. For simplicity products are grouped into phenolics, deoxygenated aromatics (DA) and cycloalkanes to show their reaction time profiles in Fig. 2(b). Based on the time evolution of these products and intermediates, the reaction scheme in Fig. 2(c) is proposed. The selectivity for phenol and benzyl phenol intermediates was observed to increase first and later decrease, whereas the selectivity for the final products increased with time (Fig. S1†). Table 1 shows the major compounds included in each of these groups and details of the final product selectivity.

As can be seen from Fig. 2(b), phenolics deoxygenation is faster without Y-zeolite but with greater formation of methylene/ethylene linked C–C dimers with partial or full hydrogenation of the benzene rings (Fig. 2(c)). The formation of such C–C dimers will be illustrated and discussed further. Interestingly, sulfided NiMoY yields higher DA due primarily to high benzene formation as shown in Table 1 for the final products. Also, even at the same selectivity for phenolics, *e.g.* ca. 40%, it can be seen in Fig. 2(b) that the selectivity for DA products was higher at 50% for NiMoY, compared to 45% for NiMoA. The results in Table 1 indicate that dimer (phenolics or DA) formation after full reaction time is significantly lower on NiMoY owing to promoted C_{aryl}–C_{aliphatic} bond cleavage of the benzyl phenols, diphenylmethane (DPM), bibenzyl (BB) and others. This facilitates the formation of monoaromatics comprising cresols, benzene, toluene and xylene (BTX). Güvenatam *et al.*³⁴ reported that acidic conditions lower the side reactions to dimers/trimers in the presence of H₂ during HDO of BPE on Pt/C. H₂-driven cracking of benzyl phenols, DPM and BB was previously reported for Fe, Ni and Mo-based catalysts at elevated temperatures and pressures.^{32,58} Koyama *et al.*³² reported considerable dimer formation while hydrocracking lignin dimers (BPE, diphenyl ether, benzyl phenols, diphenylmethane and dibenzyl) without solvent in a temperature range of 340–450 °C. The extent of C–C cleavage reported for DPM and BB was low at 420 °C but significant for BB at 450 °C. In this study no C–C cleavage of the yielded dimers was observed for NiMoA; however it was observed to a small extent on NiMoAY. Indeed, an increased selectivity for dimer products was observed for NiMoA (*discussed in the section 'Catalytic properties related to the activity'*), whereas for NiMoY the selectivity for these products peaked at 1 h and then declined. Improved C–C bond cleavage with NiMoY

opens up the possibility to valorize technical lignin in bio-refinery processes.⁴⁰

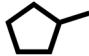





Interestingly, a high hydrogenation activity yields more cycloalkanes over sulfided NiMoA than NiMoY (Fig. 2(b)). For example, 38% cyclohexane is found for NiMoA, while it is <1% for NiMoY, which instead produced 35% benzene. Methyl-cyclopentane observed primarily with NiMoAY and NiMoY (Table 1) indicates the greater isomerization activity of these catalysts due to the higher concentration of Brønsted acidic sites in the zeolite pores promoting greater isomerization activity.⁵⁹

HDO of PPE

Fig. 3 shows the formation of phenolics, DA and alicyclics during the HDO of PPE. H₂-driven hydrogenolysis of the sp³ C–O bond (β-O-4) to ethylbenzene and phenol is fastest in this case over NiMoAY, whereas the rate of conversion of PPE is slowest for NiMoY as shown in Fig. 3(a). The details of the final product selectivity are shown in Table 2. Fig. 3(c) illustrates all of the observed components in a proposed reaction scheme. Similar to the case of BPE, note however that the phenethyl alcohol (faint print in Fig. 3(c)) intermediate that would be consumed by the recombination reactions was not detected. Transalkylation of the phenethyl group of PPE and recombination reactions are favored in the order of NiMoY > NiMoAY > NiMoA, leading to the formation of high quantities of phenolic dimers as mainly phenylethyl phenols having ethylene linked C–C bonds (Fig. 3(c)). Like with BPE, such dimers undergo C–C cleavage over NiMoY to yield ethyl phenols. The formation and cleavage of such C–C dimers will be further compared in the section '*Catalytic properties related to the activity*'. However, deoxygenated aromatics including benzene, toluene, ethylbenzene and a small number of dimers (Fig. 3(b) and Table 2) increase as the reaction progresses. Based on the evolution of these products and intermediates (Fig. S2†), a reaction scheme shown in Fig. 3(c) is proposed.

Clearly, the degree of HDO selectivity is very high with NiMoA, whereas isomerization and hydrocracking increase with NiMoY/AY. Hydrogenation activity seems lower for NiMoY leading to high monoaromatics selectivity (>80%) as with BPE, however at the expense of an even lower rate of conversion of phenolics compared to BPE (Fig. 3(b)). Noticeably, as shown in Table 2, selectivity for cycloalkane products is almost four times

Table 1 Product selectivity's from HDO of BPE after a 6 h reaction at 5 MPa and 593 K^a

Catalyst	X _{BPE} (%)	Carbon balance (%)	Selectivity (%)									
			Cycloalkanes			Deoxygenated aromatics (DA)				Phenolics		
					Others				Dimers		Cresols	Dimers
NiMoA	>99	94	<1	38	1	—	43	—	9	7	—	2
NiMoAY	>99	92	2.7	28	3.5	—	44	0.5	5	13	2	0.7
NiMoY	>99	87	9.3	<1	4.5	35	22	2	—	18	8	0.4

^a X_{BPE} refers to BPE conversion.



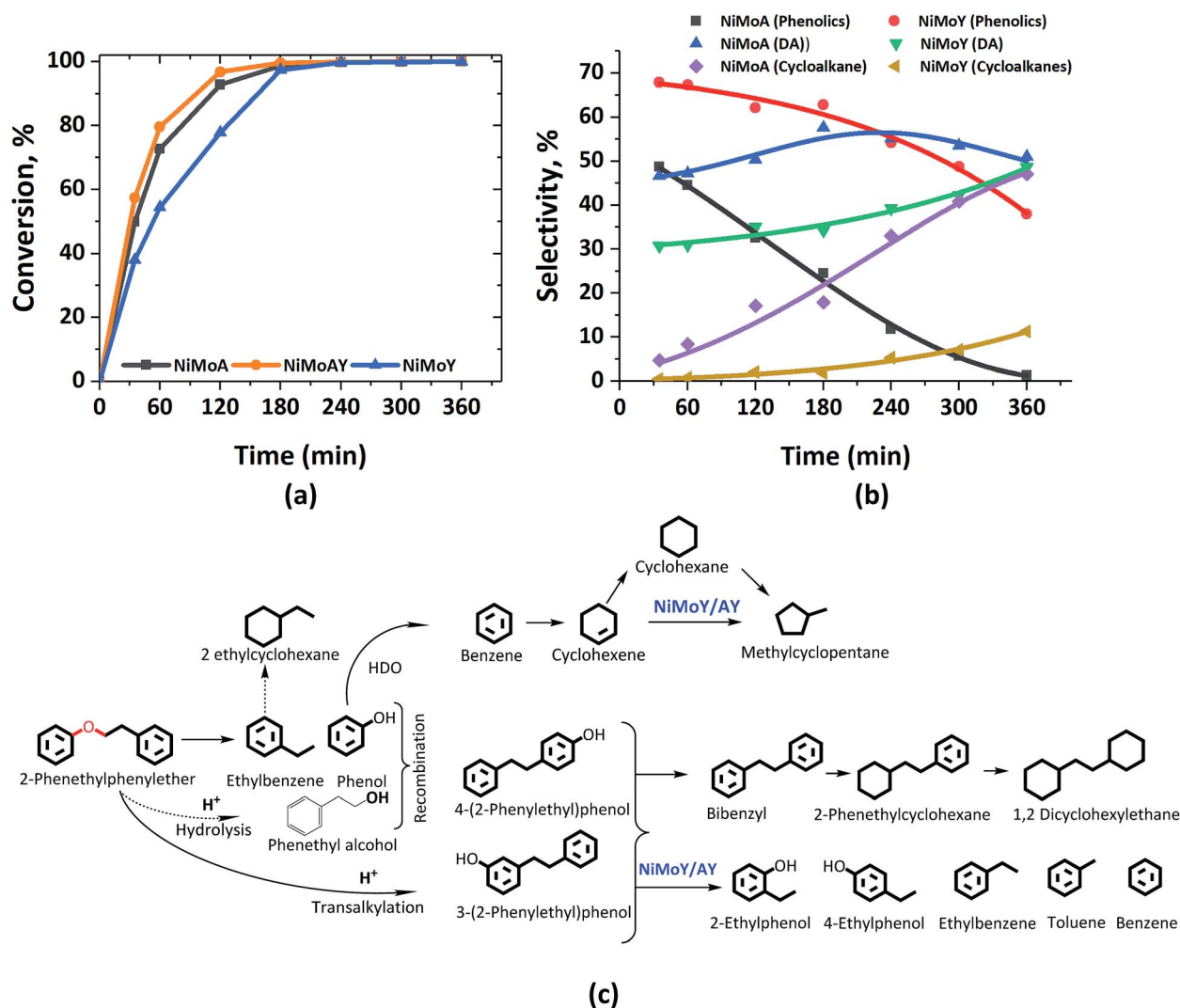


Fig. 3 (a) PPE conversion and (b) product selectivity during HDO of PPE in an autoclave at 593 K, 5 MPa and 1000 rpm. (c) Proposed reaction scheme. DA = deoxygenated aromatics.

lower with NiMoY due to a noteworthy drop in hydrogenation activity compared to NiMoA.

Compared to BPE, the cleavage of PPE and PPE derived-dimers seems hindered by the USY pore sizes, particularly its micropores. The presence of such bulkier molecules may hinder

the monophenol HDO due to preferential adsorption of the reactant/intermediates which may aid undesirable secondary reactions to build carbonaceous deposits that can deactivate the catalyst with increasing reaction time.

Table 2 Product selectivity's from HDO of PPE after a 6 h reaction at 5 MPa and 593 K^a

Catalyst	X_{PPE} (%)	Carbon balance (%)	Selectivity (%)									
			Cycloalkanes			Deoxygenated aromatics (DA)				Phenolics		
					Others				Dimers		Ethyl-phenols	Dimers
NiMoA	>99	95	—	45	3	—	—	48	3	1	—	1
NiMoAY	>99	93	17	16	3	—	—	48	3	12.5	—	3
NiMoY	>99	84	10	—	1.5	14	1	32.5	2	31	4	4

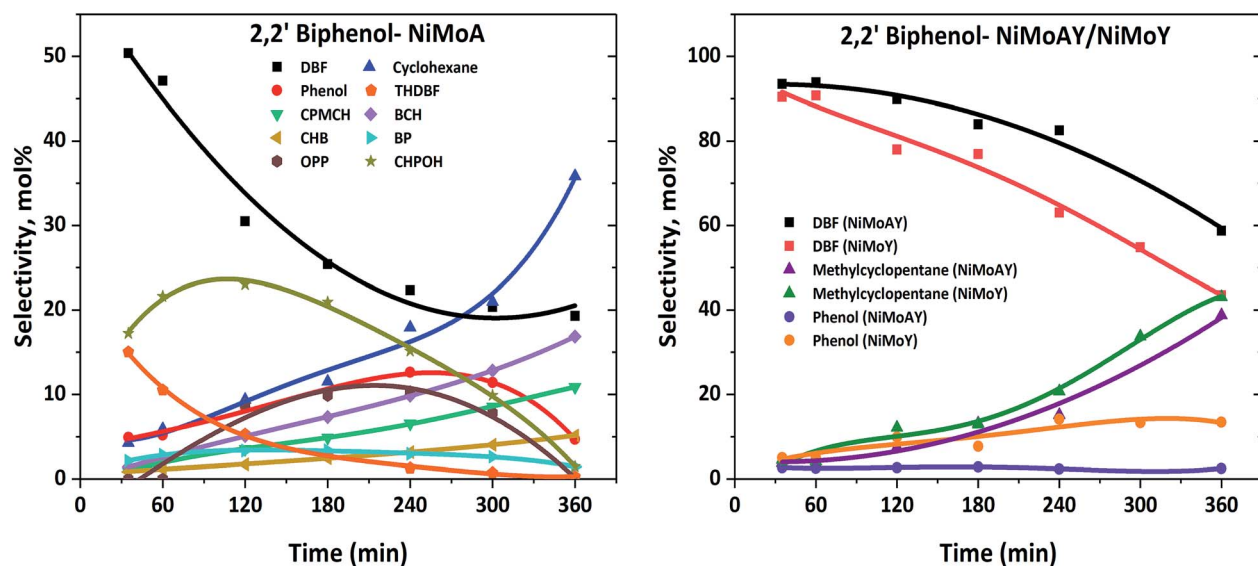
^a X_{PPE} refers to PPE conversion.

For the Y-based catalysts, the dehydration reaction is strongly favoured over DDO resulting in a high yield of DBF which is over 44%, compared to 23% with NiMoA (Table 3). As Fig. 4(a) shows that the conversion of 2,2'-biphenol to DBF occurs quickly and was complete already during the process of heating the reactor to 593 K. Also, for the Y-based catalysts, no OPP was identified in the early samples taken during the experiments. However, the cleavage of the C-O bond in the recalcitrant DBF seems to become the rate determining step, particularly for the Y-zeolite containing catalysts. Once the C-O

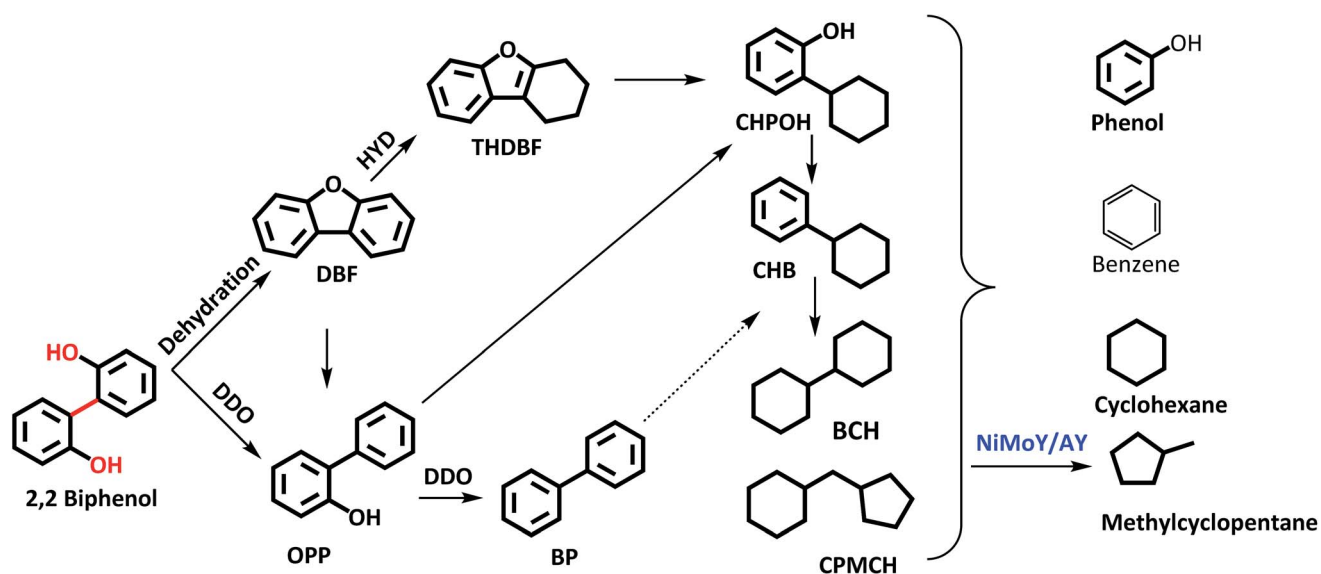
In summary, with the zeolite-based catalysts the initial formation of DBF was almost exclusively favoured, due to the stronger acidity of these catalysts promoting dehydration reactions, whereas with NiMoA formation of THDBF, OPP and various other products from it was also important. All catalysts had difficulty to further convert the recalcitrant DBF. As a result, for the zeolite-based catalysts the products after complete reaction time contained higher quantities of DBF; however their better activity for C–C cleavage reactions caused their products to be free of detectable amounts of dimers (Table 3).

The acidity of the catalysts was measured by ethylamine ($\text{C}_2\text{H}_5\text{NH}_2$) TPD and is presented in Fig. 5 and Table 5. An advantage of using ethylamine is that it measures the Brønsted acidity directly whereas the more common NH_3 -TPD requires

^a X_{5-5'} refers to 2,2'-biphenol conversion.



(a)



(b)

Fig. 4 (a) Product selectivity's during HDO of 2,2'-biphenol over NiMoA, NiMoAY and NiMoY and (b) proposed reaction scheme during HDO of 2,2'-biphenol.

Table 4 ICP data-metal contents on synthesized and spent catalysts

Catalyst	As-synthesized				After the BPE test		After the PPE test		After the 5-5' test	
	Mo (wt%)	Ni (wt%)	Si/Al	Ni/(Ni + Mo)	Si/Al	Ni/(Ni + Mo)	Si/Al	Ni/(Ni + Mo)	Si/Al	Ni/(Ni + Mo)
Y	—	—	15.0 ^a	—	—	—	—	—	—	—
NiMoA	13.3	4.6	—	0.26	—	0.28	—	0.26	—	0.24
NiMoAY	12.3	4.4	0.6	0.27	0.71	0.27	0.65	0.27	0.62	0.26
NiMoY	13.2	4.8	16.5	0.27	13.5	0.27	13.3	0.28	16.4	0.28

^a Zeolyst international.

additional confirmation by *e.g.* pyridine FTIR to distinguish between Brønsted and Lewis acidity.^{65–67} During the TPD, ethylamine adsorbs on a Brønsted acid site where proton (H^+) transfer occurs and forms ethylammonium ions. They undergo the Hoffman elimination reaction to form ethylene and ammonia at higher temperatures. The concentration of ethylene, which is less likely to undergo readsorption, is used here to quantify Brønsted acidity whereas desorbed ethylamine quantifies the Lewis acidity of the catalyst.⁶⁸ As seen from Fig. 5, the ethylene desorption peak appeared at different temperatures with an intense peak around 502 °C for NiMoAY and NiMoY. For NiMoA it is around 430 °C.

Peak shifting to higher temperatures can be attributed to the strength of the Brønsted acidity.⁶⁷ The ethylamine desorption peak appears in the range of 150–300 °C. As expected, the Brønsted acidity is the highest for the zeolite containing catalysts, both in strength as well as in amount, whereas there are little differences in the Lewis acidity of the catalysts (Table 5) and in addition the Lewis acid sites are only in the range of 5–10% of the total acidity.

The XRD patterns of the synthesized catalysts are presented in Fig. 6. No diffraction peak of NiO or MoO₃ crystallites was distinctly identified. These results indicate that the nickel and molybdenum are well dispersed on the catalyst. However, the inset in the upper right corner of Fig. 6 shows that the diffraction peak shifts toward lower angles after Ni and Mo impregnation in the Y-zeolite. Such a shift observed by others has been considered to result from a change in the composition or strain evolution in the structure.⁶⁹ Compressive strain development due to pore blockage by Ni and Mo impregnation can therefore not be ruled out. Also, the lower intensity of the diffraction signal for the NiMo impregnated catalysts may indicate lower crystallinity (amorphization) of the metal impregnated zeolite framework.⁵⁶

Indeed, pore blockage was indicated by changes in the textural properties of the synthesized catalysts, as shown in Table 6. In the fresh catalyst, the pore size is the lowest for NiMoY, where it decreased from 763 to 412 m² g^{−1} after impregnation with NiMo. These results are in line with the XRD results indicating strain evolution in the structure. A significant fraction of pore volume due to micropores in the NiMoY catalyst can cause diffusion limitations for dimers having molecular diameters greater than 7.4 Å. In such cases, the reaction will occur preferentially on the external surface or surfaces

Table 5 Acidity of the synthesized catalysts

Catalyst	Brønsted acidity (μmol g ^{−1})	Lewis acidity (μmol g ^{−1})
NiMoY	401	22
NiMoAY	370	25
NiMoA	258	30

accessible through mesopores. Sato *et al.*⁷⁰ showed that diphenylmethane having a molecular size of 6.2 Å can effectively access the micro- and meso-pores of Y-zeolite. Additionally, a significant reduction in mesopore sizes was observed after the catalytic activity test with all the lignin dimers due to pore blockage. Pore blockage is indeed highest with Y-based catalysts likely due to higher carbon deposition on the catalytic surfaces. For NiMoY/NiMoAY, a 30–45% reduction in the surface area occurred while for NiMoA it is about 8–20%.

Elemental analysis on the recovered catalysts gives the C, H and S contents of the sulfided and post-reaction recovered catalysts as shown in Table 7. For BPE, PPE and 2,2'-biphenol treated catalysts, the carbon deposition rises with increasing Y-zeolite content. Also, in a repeated test using the recovered NiMoY catalyst from the first run with 2,2-biphenol shows an increased carbon content (3 wt% to 5.2 wt%) on the catalyst surface. This is due to the higher concentration of Brønsted acidic sites on NiMoY leading to undesirable side reactions (*e.g.* adsorption, condensation, polymerization, *etc.*) of highly reactive adsorbed coke precursors like phenolics. This eventually contributes to catalyst deactivation as the reaction proceeds which has been reported for metal sulfide based catalysts earlier.⁷¹ The carbon depositions on the spent catalysts are normalized against the quantity of the conversion of each of the model compounds to deoxygenated products (denoted as C* in Table 7). It seems that carbon deposition is slightly higher for the conversion of the β-O-4 linkage of the model compound (PPE) with the Y-zeolite containing catalysts. This may be

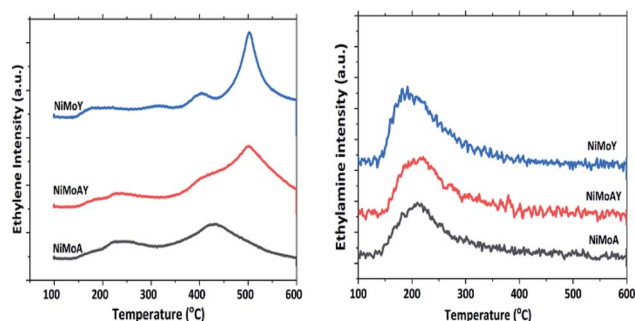


Fig. 5 Relative intensity of ethylene and ethylamine during the desorption of ethylamine-TPD.

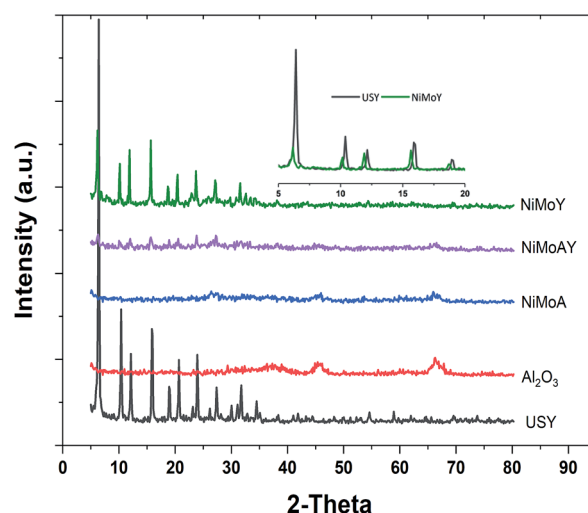
Fig. 6 XRD pattern of the synthesized catalysts, parent USY and γ-Al₂O₃.

Table 6 N₂ physisorption data for fresh and spent catalysts^a

Catalyst	As synthesized			After the BPE test			After the PPE test			After the 5-5' test		
	<i>S_a</i>	<i>V_p</i>	<i>d_p</i>	<i>S_a</i>	<i>V_p</i>	<i>d_p</i>	<i>S_a</i>	<i>V_p</i>	<i>d_p</i>	<i>S_a</i>	<i>V_p</i>	<i>d_p</i>
γ-Al ₂ O ₃	199	0.48	97.6									
USY	763	0.25	63.3									
NiMoA	139	0.31	87.6	111	0.18	84.9	119	0.20	79.1	128	0.26	78
NiMoAY	270	0.26	71.9	163	0.18	43.8	148	0.19	51.8	175	0.23	51.9
NiMoY	412	0.20	53.1	291	0.20	27.6	246	0.20	31.9	—	—	—

^a *S_a* = BET surface area (m² g⁻¹), *V_p* = pore volume (cm³ g⁻¹), and *d_p* = average pore size for mesopores (Å).

Table 7 Elemental contents of carbon, hydrogen and sulfur on the freshly sulfided and spent catalysts^a

Catalyst	Freshly sulfided			After the BPE test			After the PPE test			After the 5-5' test		
	C	H	S	C*	H	S	C*	H	S	C*	H	S
NiMoA	0.4	1.3	8.8	0.98	0.8	7.7	2.1	0.7	8.2	2.7	0.5	8.3
NiMoAY	—	—	8.3	2.1	1.5	6.2	4.0	0.6	7.8	3.7	0.4	7.0
NiMoY	1.0	0.9	9.8	6.5	1.6	7.1	7.9	0.5	8.9	6.7	0.5	7.0

^a C values for catalysts after reaction tests are in (g carbon)/(g catalyst)/(mol of feed converted to deoxygenated products). All other values are in wt% including C in the sulfide catalyst.

related to the higher diffusion resistance of the larger PPE compound in the zeolite structure compared to the other model compounds. Differences in the H content between the fresh and spent catalysts are negligible, whereas there is only a minor decrease in the S content of the spent catalysts.

Raman spectra of the synthesized catalysts are presented in Fig. 7. The main peak for all prepared catalysts appeared at around 953 cm⁻¹. This corresponds to the symmetric stretching vibration of Mo=O in octahedrally coordinated Mo oxide species which are considered to interact weakly with the support.⁷² Such weak interaction enables the formation of highly reducible species and should enhance the activity of the catalyst. Despite a slight shift of the main peak for NiMoAY, all catalysts have similar metal-support interaction. However, peak shoulders observed at different points indicate the presence of bulk MoO₃ phases (995 cm⁻¹), less active or inactive tetrahedrally coordinated Mo oxide species (900 cm⁻¹) and the Mo–O–Mo vibration of orthorhombic MoO₃, inferring the presence of polymerized Mo oxides (825 cm⁻¹). The absence of the bulk MoO₃ peak shoulder at around 995 cm⁻¹ for the more acidic supported catalysts (NiMoAY and NiMoY) implies that they contain more easily reducible Mo oxide species.

XPS analysis of the sulfided NiMoA and NiMoY is shown in Fig. 8. Evaluation of the Ni 2p and Mo 3d core level spectra infers how the support acidity influences the sulfidation of Mo and Ni. Mo 3d spectral fitting values are: Mo⁴⁺ (MoS₂) 228.7 ± 0.1 eV for Mo 3d_{5/2} and 231.9 ± 0.1 eV for Mo 3d_{3/2}; Mo⁶⁺ (MoO₃) 232.2 ± 0.1 eV for Mo 3d_{5/2} and 235.4 ± 0.1 eV for Mo 3d_{3/2}. Ni 2p spectral fitting and deconvolution show the presence of NiS_x, NiMoS and Ni²⁺ species at 852.8 ± 0.1, 854.3 ± 0.1 and 856 ± 0.2 eV binding energies respectively. Mo sulfidation was calculated

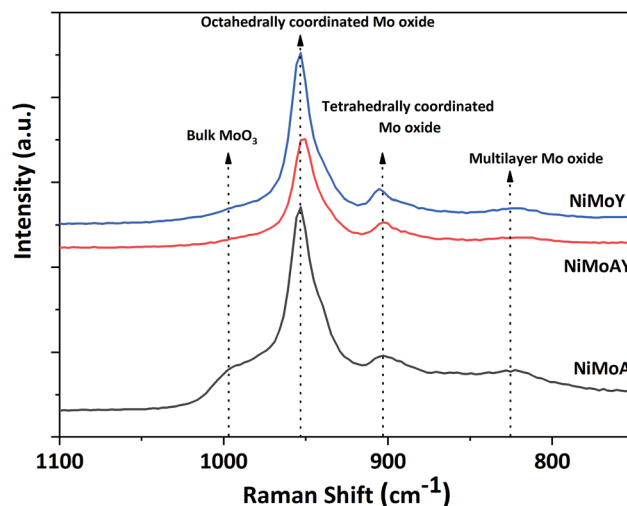


Fig. 7 Raman spectra of the synthesized catalyst.

as the contribution of Mo⁴⁺ relative to the total amount of Mo species in the Mo 3d core level spectra (excluding S 2s contribution) and Ni sulfidation as the contribution from NiS_x and NiMoS relative to the total amount of NiS_x, NiMoS and Ni²⁺. The results in Table 8 show that with the Y support, the contribution of the NiMoS phase is slightly higher than for NiMoA. This indicates that more Ni atoms are embedded into the MoS₂ slabs to form the active NiMoS phase⁷³ to a slightly better extent with the Y supported catalyst.

Overall sulfidation seems quite similar for both catalysts, and thus independent of the nature of the support. However, the degree of sulfidation may be underestimated from these results since there is a risk for some superfluous oxidation while transferring samples to the XPS chamber.

The morphologies of the metal sulfides are crucial in determining their activity and selectivity under the reaction conditions. The HRTEM images of the sulfided NiMoA and NiMoY shown in Fig. 9 revealed the dispersion of the active NiMoS phase. The average values of the slab length, number of stacks/slabs and fraction of edge Mo atoms were calculated based on 300 individual MoS₂ crystals for each sample. As seen from Table 8, a shorter slab length and higher stacking degree with the Y zeolite increase the dispersion (*f_{Mo}*) of the active phases compared to NiMoA. This means that more edge and corner sites of Mo atoms shall be accessible for the case with NiMoY.



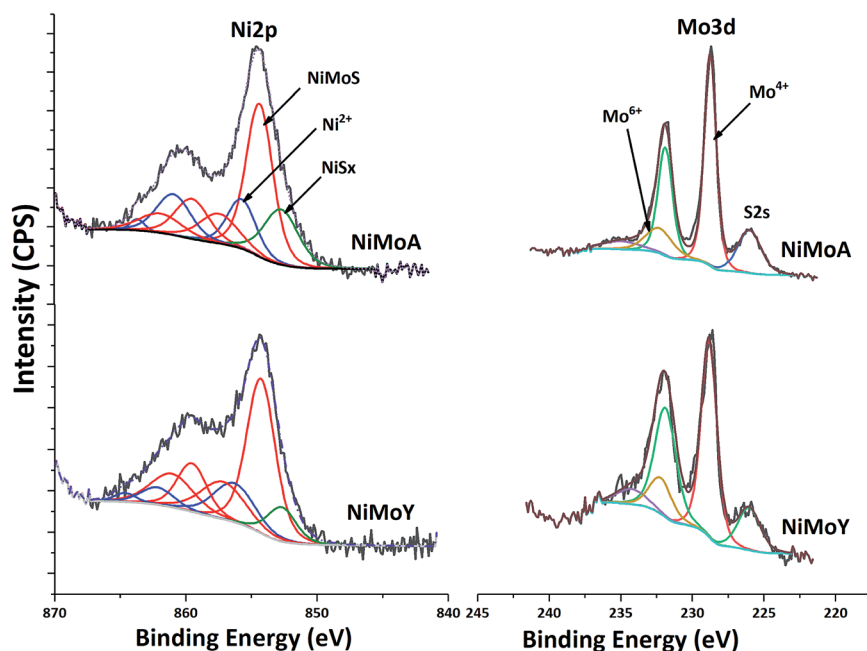


Fig. 8 Core level XPS spectra of Ni 2p and Mo 3d for NiMoA and NiMoY.

Catalytic properties related to the activity

The characterization of the catalysts *via* TEM, Raman and XPS revealed that NiMo on Y has more active Mo species than NiMoA, due mainly to less bulk MoO₃ leading to a comparable degree of sulfidation and an improved dispersion of the active phase. Also, ethylamine-TPD showed a higher concentration of Brønsted acidity on the Y supported catalysts. This provided an enhanced hydrogenolysis of the ether linkage of BPE over NiMoY. However, for PPE the rate of hydrogenolysis is lower for the pure Y supported catalyst. Indeed, for both BPE and PPE, hydrogenolysis is faster on the mixed-support catalyst (NiMoAY) with moderate Brønsted acidity as shown in Fig. 2(a) and 3(a). However, for both cases transalkylation, recombination and acid catalyzed condensation of intermediates were significant leading to the formation of stable aliphatic C-linked phenolic/deoxygenated dimers (Fig. 2(c) and 3(c)). An acid catalyzed intramolecular dehydration reaction was also dominant for 2,2'-biphenol HDO. The combination and proximity of Mo dispersion and Brønsted acidity on NiMoY seem able to effectively cleave the intermediate C-C dimers (both deoxygenated and phenolic). Enhanced hydrocracking for BPE derived intermediates (*e.g.* DPM, BB, benzyl phenols *etc.*) to monophenols (cresols) and BTX thus leads to fewer residual dimers. PPE

derived intermediates also undergo such cracking to ethyl phenols. For 2,2'-biphenol almost no intermediate C-C dimers remained. It is also evident that methyl cyclopentane is a dominant product in the case of NiMoY for all three reactants which indicates the higher isomerization activity of this catalyst. However, the activity tests revealed that the deoxygenation/hydrogenation activity for NiMoY was lower compared to that of NiMoA/NiMoAY. This has led to different products consisting of a mixture of deoxygenated products and cycloalkanes over NiMoA while more aromatics over NiMoY for BPE, PPE and 2,2'-biphenol. The possible reasons for these differences proposed in the literature based on studies of hydroprocessing with sulfided metals on Y zeolite include: (1) stronger adsorption of oxygenates and phenolics on the zeolite surface creating a surface pool of these species, (2) inaccessibility of acidic sites in smaller micropores, (3) the longer diffusion distance between the metallic and acidic sites, *i.e.* poorer proximity of the active sites especially for the micropores of the zeolite, and (4) different morphologies of metal sulfides inside the zeolite micropores.^{74,75}

Previous studies from our group showed that the average particle size of NiMo on alumina, AY and Y-zeolite was in the range of 180–310 Å, which is much larger than that of the zeolite

Table 8 XPS and TEM characterization of the metal sulfides

Catalyst	Mo sulfidation (%)		Ni sulfidation (%)			Slab length (nm)	Stacking	f_{Mo}
	Mo ⁴⁺		NiS _x	NiMoS	Ni ²⁺			
NiMoA	84		16	54	30	4.7	3.8	0.22
NiMoY	82		8	61	31	4.1	4.2	0.27



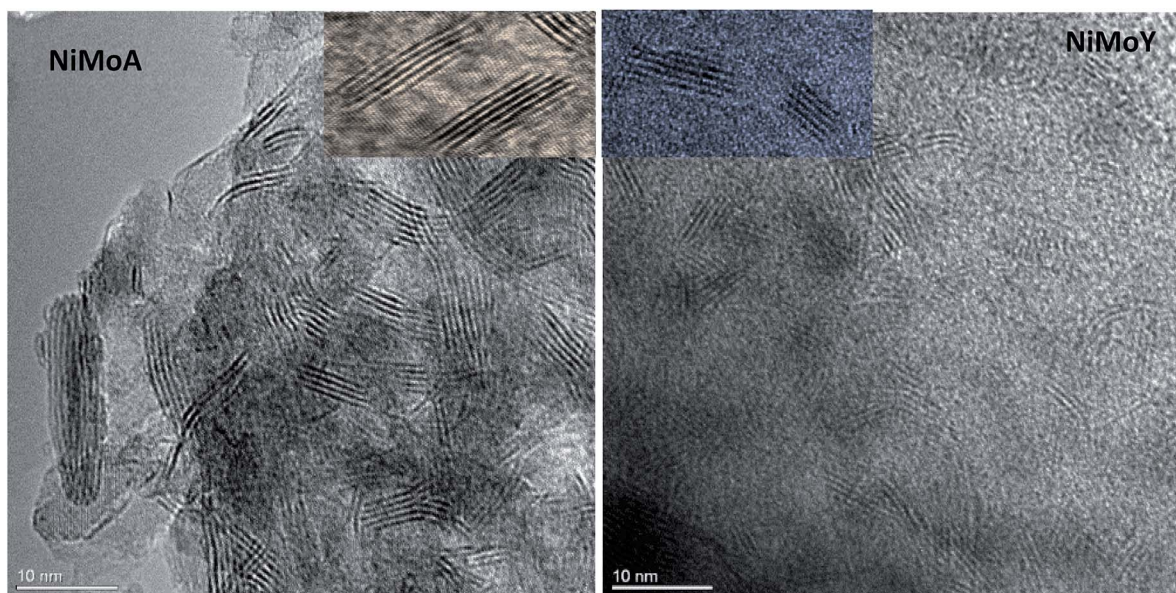


Fig. 9 Characteristic HRTEM images of NiMoA and NiMoY: insets show the differences in slab distribution.

supercage of 12 Å.⁵⁵ This implies that a portion of particles will remain at the grain boundaries on the external surfaces of the micropore, but parts could be inside the grain and may even not be sulfided.⁷⁶ The fraction inside grains will be less accessible to the reactants/intermediates. Fig. 10(a) shows the yield of the intermediate phenolic dimers formed during HDO of BPE and PPE over NiMoA and NiMoY. These phenolic dimers are formed from transalkylation and recombination reactions as discussed above. First it can be noted that for the PPE feed the yields of phenolic dimers (2-phenylethylphenols) are higher for NiMoY during the entire reaction period (Fig. 10(a)), whereas for BPE the phenolic dimers (benzyl phenols) are only initially higher for NiMoY. This is likely due to the greater acidity of NiMoY catalyzing transalkylation and dehydration/condensation

reactions to form more dimers. For BPE, the intermediate benzyl phenol dimers reached a lower peak yield indicating that they could be converted more rapidly as they should be more accessible to the zeolite micropores than PPE dimers to be cracked to form smaller molecules. For PPE, the formation of 2-phenylethylphenol dimers showed a peak of higher maximum yield after around 3 h, which corresponds to when all the PPE has converted (see Fig. 3(a)), followed by a steep decrease. This indicates that the diffusion limitations play a role for both BPE and PPE; however they are more prominent for PPE and its dimers due to their larger molecular size. The diffusion limitations and pore mouth blockage create a larger surface phenolics pool. As noticed, the degree of hydrocracking/deoxygenation increases over NiMoY once the BPE/PPE are converted.

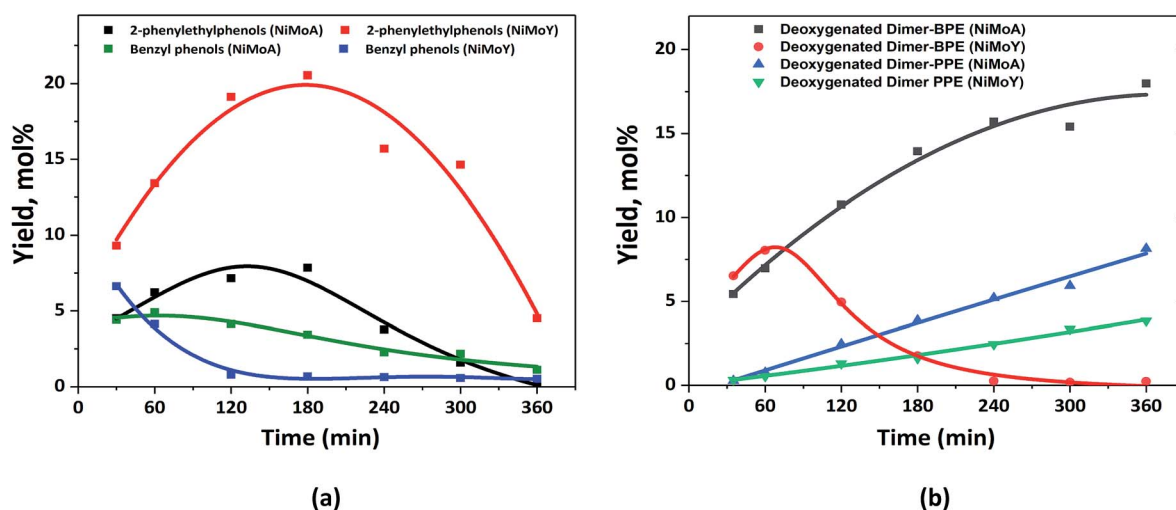


Fig. 10 (a) Yield of the intermediate phenolic dimers and benzyl phenols from BPE and 2-phenylethylphenols from PPE; (b) deoxygenated dimers from BPE and PPE.



its higher initial activity for the formation of phenolic dimers and diffusion limitations. Also, a higher rate of coke formation was observed for the Y-based catalyst which may lead to faster catalyst deactivation. Hence, the proximity of the deoxygenation and acidic sites and their accessibility to the reactant/intermediates likely plays a key role for the product selectivity during HDO on NiMo based catalysts on Y-zeolites.

Conflicts of interest

Acknowledgements

This work is performed at the Competence Centre for Catalysis (KCK) and division of chemical reaction engineering at the Chalmers University of Technology. We would like to acknowledge the Swedish Energy Agency (contract: 2016-08330) for the financial aid. We would also like to acknowledge Stefan Gustafsson for his help with the TEM analysis.

Notes and references

- ## Conclusions

Sustainable Energy Fuels, 2020, 4, 149–163 | 161

- 16 D. Shi, L. Arroyo-Ramírez and J. M. Vohs, *J. Catal.*, 2016, **340**, 219–226.
- 17 V. N. Bui, D. Laurenti, P. Afanasiev and C. Geantet, *Appl. Catal., B*, 2011, **101**, 239–245.
- 18 I. D. Mora, E. Méndez, L. J. Duarte and S. A. Giraldo, *Appl. Catal., A*, 2014, **474**, 59–68.
- 19 I. D. Mora-Vergara, L. Hernández Moscoso, E. M. Gaigneaux, S. A. Giraldo and V. G. Baldovino-Medrano, *Catal. Today*, 2018, **302**, 125–135.
- 20 Z. He, M. Hu and X. Wang, *Catal. Today*, 2018, **302**, 136–145.
- 21 Z. Luo, Z. Zheng, Y. Wang, G. Sun, H. Jiang and C. Zhao, *Green Chem.*, 2016, **18**, 5845–5858.
- 22 X. Zhang, T. Wang, L. Ma, Q. Zhang, Y. Yu and Q. Liu, *Catal. Commun.*, 2013, **33**, 15–19.
- 23 E. Laurent and B. Delmon, *Appl. Catal., A*, 1994, **109**, 97–115.
- 24 X. Lan, E. J. M. Hensen and T. Weber, *Appl. Catal., A*, 2018, **550**, 57–66.
- 25 H. Y. Zhao, D. Li, P. Bui and S. T. Oyama, *Appl. Catal., A*, 2011, **391**, 305–310.
- 26 T. R. H. Douglas and C. Elliott, *Energy Fuels*, 2009, **23**, 631–637.
- 27 M. Alda-Onggar, P. Maki-Arvela, K. Eranen, A. Aho, J. Hemming, P. Paturi, M. Peurla, M. Lindblad, I. L. Simakova and D. Y. Murzin, *ACS Sustainable Chem. Eng.*, 2018, **6**, 16205–16218.
- 28 X. Liu, W. Jia, G. Xu, Y. Zhang and Y. Fu, *ACS Sustainable Chem. Eng.*, 2017, **5**, 8594–8601.
- 29 P. E. Ruiz, B. G. Frederick, W. J. De Sisto, R. N. Austin, L. R. Radovic, K. Leiva, R. García, N. Escalona and M. C. Wheeler, *Catal. Commun.*, 2012, **27**, 44–48.
- 30 X. Li, G. Chen, C. Liu, W. Ma, B. Yan and J. Zhang, *Renewable Sustainable Energy Rev.*, 2017, **71**, 296–308.
- 31 M. Saidi, F. Samimi, D. Karimipourfard, T. Nimmanwudipong, B. C. Gates and M. R. Rahimpour, *Energy Environ. Sci.*, 2014, **7**, 103–129.
- 32 M. Koyama, *Bioresour. Technol.*, 1993, **44**, 209–215.
- 33 A. L. Jongerius, R. Jastrzebski, P. C. A. Bruijninx and B. M. Weckhuysen, *J. Catal.*, 2012, **285**, 315–323.
- 34 B. Güvenatam, O. Kurşun, E. H. J. Heeres, E. A. Pidko and E. J. M. Hensen, *Catal. Today*, 2014, **233**, 83–91.
- 35 C. Zhao and J. A. Lercher, *Angew. Chem., Int. Ed.*, 2012, **51**, 5935–5940.
- 36 W. Zhang, J. Chen, R. Liu, S. Wang, L. Chen and K. Li, *ACS Sustainable Chem. Eng.*, 2014, **2**, 683–691.
- 37 Y.-K. Hong, D.-W. Lee, H.-J. Eom and K.-Y. Lee, *Appl. Catal., B*, 2014, **150–151**, 438–445.
- 38 W. Schutyser, T. Renders, S. Van den Bosch, S. F. Koelewijn, G. T. Beckham and B. F. Sels, *Chem. Soc. Rev.*, 2018, **47**, 852–908.
- 39 W. Song, S. Zhou, S. Hu, W. Lai, Y. Lian, J. Wang, W. Yang, M. Wang, P. Wang and X. Jiang, *ACS Catal.*, 2018, **9**, 259–268.
- 40 L. Shuai, J. Sitison, S. Sadula, J. Ding, M. C. Thies and B. Saha, *ACS Catal.*, 2018, **8**, 6507–6512.
- 41 S. Mukundan, L. Atanda and J. Beltramini, *Sustainable Energy Fuels*, 2019, **3**, 1317–1328.
- 42 M. Williams, B. Fonfe, C. Sievers, A. Abraham, J. Vanbokhoven, A. Jentys, J. Vanveen and J. Lercher, *J. Catal.*, 2007, **251**, 485–496.
- 43 J. García-Martínez, M. Johnson, J. Valla, K. Li and J. Y. Ying, *Catal. Sci. Technol.*, 2012, **2**, 987–994.
- 44 Z. Ma, E. Troussard and J. A. van Bokhoven, *Appl. Catal., A*, 2012, **423–424**, 130–136.
- 45 J. Garcia-Martinez, K. Li and G. Krishnaiah, *Chem. Commun.*, 2012, **48**, 11841–11843.
- 46 S. G. A. Ferraz, B. M. Santos, F. M. Z. Zotin, L. R. R. Araujo and J. L. Zotin, *Ind. Eng. Chem. Res.*, 2015, **54**, 2646–2656.
- 47 S. G. A. Ferraz, F. M. Z. Zotin, L. R. R. Araujo and J. L. Zotin, *Appl. Catal., A*, 2010, **384**, 51–57.
- 48 J.-I. Park, J.-K. Lee, J. Miyawaki, Y.-K. Kim, S.-H. Yoon and I. Mochida, *Fuel*, 2011, **90**, 182–189.
- 49 M. O. Kazakov, K. A. Nadeina, I. G. Danilova, P. P. Dik, O. V. Klimov, V. Y. Pereyma, E. A. Paukshtis, I. S. Golubev, I. P. Prosvirin, E. Y. Gerasimov, I. V. Dobryakova, E. E. Knyazeva, I. I. Ivanova and A. S. Noskov, *Catal. Today*, 2019, **329**, 108–115.
- 50 D. Y. Hong, S. J. Miller, P. K. Agrawal and C. W. Jones, *Chem. Commun.*, 2010, **46**, 1038–1040.
- 51 H. Lee, H. Kim, M. J. Yu, C. H. Ko, J. K. Jeon, J. Jae, S. H. Park, S. C. Jung and Y. K. Park, *Sci. Rep.*, 2016, **6**, 28765.
- 52 A. K. Deepa and P. L. Dhepe, *RSC Adv.*, 2014, **4**, 12625–12629.
- 53 M. Abdus Salam, D. Creaser, P. Arora, S. Tamm, E. Lind Grennfelt and L. Olsson, *Catalysts*, 2018, **8**, 418.
- 54 P. Arora, H. Ojagh, J. Woo, E. Lind Grennfelt, L. Olsson and D. Creaser, *Appl. Catal., B*, 2018, **227**, 240–251.
- 55 H. Ojagh, D. Creaser, M. A. Salam, E. L. Grennfelt and L. Olsson, *Fuel Process. Technol.*, 2019, **190**, 55–66.
- 56 W. Zhou, Y. Zhou, Q. Wei, L. Du, S. Ding, S. Jiang, Y. Zhang and Q. Zhang, *Chemistry*, 2017, **23**, 9369–9382.
- 57 J. He, L. Lu, C. Zhao, D. Mei and J. A. Lercher, *J. Catal.*, 2014, **311**, 41–51.
- 58 X.-Y. Wei, E. Ogata, Z.-M. Zong and E. Niki, *Energy Fuels*, 1992, **6**, 868–869.
- 59 W.-C. Cheng and K. Rajagopalan, *J. Catal.*, 1989, **119**, 354–358.
- 60 S. Krishnamurthy, S. Panvelker and Y. T. Shah, *AIChE J.*, 1989, **27**, 994–1001.
- 61 J. Zhang, C. Li, X. Chen, W. Guan and C. Liang, *Catal. Today*, 2019, **319**, 155–163.
- 62 J. Zhang, C. Li, X. Chen, Y. Chen, L. Zhang, B. Zhang and C. Liang, *J. Catal.*, 2019, **371**, 346–356.
- 63 J. Zhang, L. Wang, C. Li, S. Jin and C. Liang, *Org. Process Res. Dev.*, 2018, **22**, 67–76.
- 64 L. Wang, H. Wan, S. Jin, X. Chen, C. Li and C. Liang, *Catal. Sci. Technol.*, 2015, **5**, 465–474.
- 65 O. A. Abdelrahman, K. P. Vinter, L. Ren, D. Xu, R. J. Gorte, M. Tsapatsis and P. J. Dauenhauer, *Catal. Sci. Technol.*, 2017, **7**, 3831–3841.
- 66 O. Kresnawahjuesa, R. J. Gorte, D. d. Oliveira and L. Y. Lau, *Catal. Lett.*, 2002, **82**, 155–160.
- 67 R. J. Gorte, *Catal. Lett.*, 1999, **62**, 1–13.
- 68 H. H. Ingelsten, M. Skoglundh and E. Fridell, *Appl. Catal., B*, 2003, **41**, 287–300.



- 69 A. Wang, B. Lin, H. Zhang, M. H. Engelhard, Y. Guo, G. Lu, C. H. F. Peden and F. Gao, *Catal. Sci. Technol.*, 2017, **7**, 2362–2370.
- 70 K. Sato, Y. Nishimura and H. Shimada, *Catal. Lett.*, 1999, **60**, 83–87.
- 71 O. İ. Şenol, T. R. Viljava and A. O. I. Krause, *Appl. Catal., A*, 2007, **326**, 236–244.
- 72 N. Kunisada, K.-H. Choi, Y. Korai, I. Mochida and K. Nakano, *Appl. Catal., A*, 2004, **269**, 43–51.
- 73 W. Zhou, M. Liu, Q. Zhang, Q. Wei, S. Ding and Y. Zhou, *ACS Catal.*, 2017, **7**, 7665–7679.
- 74 E. J. M. Hensen and J. A. R. van Veen, *Catal. Today*, 2003, **86**, 87–109.
- 75 K. Sato, Y. Nishimura, K. Honna, N. Matsubayashi and H. Shimada, *J. Catal.*, 2001, **200**, 288–297.
- 76 M. J. M. Leglise, C. Potvin, G. Djega-Mariadassou and D. Cornet, *J. Catal.*, 1995, **152**, 275–290.
- 77 M. Heuchel, C. Dörr, R. Boldushevskii, S. Lang, E. Klemm and Y. Traa, *Appl. Catal., A*, 2018, **553**, 91–106.

